Conformational Role of the Divalent Metal in Bovine Heart Mitochondrial F1-ATPase: An Electron Spin Echo Envelope Modulation Study†

Alfonso Zoleo,‡ Giovanna Lippe,§,|| Stefania Contessi,§,|| Marina Brustolon,‡ Federica Dabbeni-Sala,*,⊥ and Anna Lisa Maniero*,‡

Department of Chemistry, University of Padova, via Marzolo 1, and Department of Pharmacology, University of Padova, largo Meneghetti 2, I-35131 Padova, and Department of Biomedical Sciences and Technologies and MATI Center of Excellence, University of Udine, P.le Kolbe 4, I-33100 Udine, Italy

Received May 17, 2007; Revised Manuscript Received July 23, 2007

ABSTRACT: The catalytic sites of beef heart mitochondrial F1-ATPase were studied by electron spin echo envelope modulation (ESEEM) spectroscopy, using Mn(II) as a paramagnetic probe, which replaces the naturally occurring Mg(II), maintaining the enzyme catalytic activity. F1-ATPase was purified from beef heart mitochondria. A protein still containing three endogenous nucleotides, named MF1(1,2), is obtained under milder conditions, whereas a harsher treatment gives a fully depleted F1, named MF1(0,0). Several samples were prepared, loading MF1(0,0) or MF1(1,2) with Mn(II) or Mn^{II}ADP in both substoichiometric and excess amounts. When MF1(1,2) is loaded with Mn(II) in a 1:0.8 ratio, the FT-ESEEM spectrum shows evidence of a nitrogen interacting with the metal, while this interaction is not present in MF1(0,0) + Mn(II) in a 1:0.8 ratio. However, when MF1(0,0) is loaded with 2.4 Mn(II), the FT-ESEEM spectrum shows a metal−nitrogen interaction resembling that present in MF1(1,2) + Mn(II) in a 1:0.8 ratio. These results strongly support the role of the metal alone in shaping and structuring the catalytic sites of the enzyme. When substoichiometric ADP is added to MF1(1,2) preloaded with 0.8 equiv of Mn(II), the ESEEM spectra show evidence of a phosphorus nucleus coupled to the metal, indicating that the nucleotide phosphate binding to Mn(II) occurs in a catalytic site. Generally, ^{14}N coordination to the metal is clearly identified in the ESEEM spectra of all the samples containing more than one metal equivalent. One point of note is that the relevant nitrogen-containing ligand(s), responsible for the signals in the ESEEM spectra, has not yet been identified in the available X-ray structures.

Mitochondrial ATP synthase is composed of a membrane portion named F0 and a soluble portion named F1. The two parts are connected structurally and functionally by the peripheral stalk, which organizes the stator and the central rotor: the synthesis and hydrolysis of ATP are driven by the rotation of this rotor (*1*−*3*). The F1 portion contains six nucleotide-binding sites, three of which, located in the β subunits, are catalytic, and the other three, located in the α subunits, do not exchange nucleotides during catalysis and are referred to as noncatalytic sites. Many X-ray structures are available, obtained for crystals of the bovine heart F1, grown under different conditions, mirroring different functional states (*4*−*6*). In 1993 Boyer proposed a mechanism for the catalysis known as the binding change mechanism (*7*), which requires that the three catalytic sites are in a different conformation at any given time. During catalysis, they interconvert sequentially among the different conformations, by the rotation of the central stalk with respect to the $\alpha_3\beta_3$ subcomplex. Boyer's model is commonly accepted, but the number of states for a single catalytic subunit is still debated (*8*, *9*). Another open question is the role of Mg^{2+} in the catalysis. It is well-known that the true substrates, in both synthesis and hydrolysis of ATP, are Mg−nucleotide complexes, and not just the nucleotides. As elegantly demonstrated by Senior for *E. coli* F1-ATPase (*10*, *11*), the Mg(II)−nucleotide complexes bound to the enzyme are strategic in inducing the asymmetry of the catalytic sites necessary for the sequential enzyme cycle: in fact, only in the presence of Mg^{2+} is pronounced binding cooperation among the three catalytic sites observed. The aim of our work is to highlight the role of the metal ion or of the metal ion−nucleotide complex in the sequential catalysis.

The F1 portion from bovine heart can be isolated, maintaining its hydrolytic activity, by the use of milder or harsher conditions. The purified enzyme preparations do not show any difference in the subunit composition, as demonstrated by identical electrophoretic patterns, but differ in the content of bound nucleotides (*12*).

We used two differently purified enzymes: more harshly purified F1-ATPase not retaining any nucleotides, named F1-(0,0), and a more mildly purified F1-ATPase, named F1-

† This work was supported by the University of Padova through the project "Studio con risonanze di Spin elettronico dell'enzima F1" (Cdr. A.0EE00.96) and by Regione Friuli Venezia Giulia (legge regionale 11/2003).

* To whom correspondence should be addressed. (F.D.-S.) E-mail: federica.dabbenisala@unipd.it. Phone: 0039 49 8275096. Fax: +39-049-8275093. (A.L.M.) E-mail: annalisa.maniero@unipd.it. Phone: 0039 49 8275109. Fax: +39-049-8275239.

‡ Department of Chemistry, University of Padova.

§ Department of Biomedical Sciences and Technologies, University of Udine.

|| MATI Center of Excellence, University of Udine.

⊥ Department of Pharmacology, University of Padova.

10.1021/bi700949e CCC: $37.00
Published on Web 10/26/2007

(1,2), which contains an average of two noncatalytic sites occupied by tightly bound nucleotides and one catalytic site occupied by a Mg(II)−nucleotide complex (*12*). The involvement of the metal ion in constructing and maintaining the conformation of a potentially competent catalytic site is studied by using ESEEM[1] spectroscopy. Mn^{2+}, a paramagnetic ion that replaces Mg^{2+}, maintaining the catalytic activity, has been used, as in previous successful studies of F1 from mammals, chloroplasts, and bacteria (*13*−*17*). Mn^{2+} has been added both alone and as a metal−nucleotide complex to each of the two purified enzymes. Our results clearly show that the metal ion alone plays a central role in shaping a competent catalytic site.

EXPERIMENTAL PROCEDURES

Purification of MF1(1,2) and MF1(0,0). Salts and buffers were from Sigma-Aldrich. ATP and ADP were from ICN. Pure soluble MF1 was prepared from beef heart mitochondria as in ref *18* or as in ref *19*, precipitated in ammonium sulfate at 50%, and stored at 4 °C in the presence of 4 mM Na/ATP.

The enzyme MF1(0,0), fully depleted of nucleotides and magnesium, was obtained according to ref *19* in a buffer containing 100 mM Tris/SO_4, 4 mM EDTA, and glycerol, 50% (v/v), at pH 8 starting from MF1 purified as in ref *19*. The enzyme fractions with $A_{280}/A_{260} > 1.9$, which contain less than 0.2 mol of nucleotides/mol of MF1, were collected, pulled together, and stored at −20 °C.

MF1(1,2) was prepared from MF1 by removing loosely bound nucleotides. An aliquot of protein stored at 4 °C in ammonium sulfate at 50% was centrifuged, resuspended in 20 mM HEPES−KOH, pH 8, loaded onto a centrifugation−gel filtration column, and concentrated by microconcentrators, if necessary. The enzyme contained 2.8 ± 0.1 mol of tightly bound nucleotides (mainly ADP), assayed by HPLC analyses on a strong anion-exchange column (Partisil SAX-10, Whatman), as in ref *20*.

The enzyme purity and the subunit stoichiometric composition of each preparation were determined by SDS−PAGE (*21*).

Enzyme activity was monitored as described in ref *20*.

EPR Sample Preparation. $MnSO_4 \cdot H_2O$ (ACS reagent, purity 98%) was from Aldrich. A 1 mM solution of Mn^{2+} was freshly prepared by dissolving $MnSO_4 \cdot H_2O$ in HEPES−KOH buffer. A 1 mM ADP stock solution was prepared by dissolving ADP in HEPES−KOH buffer. Aliquots of MF1-(0,0) for EPR were obtained from the dilution of the glycerol buffer containing the concentrated protein that had been stored at −20 °C. The dilution of the protein was carried out in a 20 mM HEPES−KOH plus 20% glycerol (v/v) buffer, pH 8, at room temperature. Aliquots of MF1(1,2) for EPR were freshly prepared from MF1 as reported in the previous section. The enzyme final concentration was 35 μM in all EPR samples. Suitable small volumes of Mn(II) solution and, in some cases, of ADP solution were added to the protein aliquots to form the EPR samples with the wanted metal:nucleotide:protein ratios. The samples were transferred in the EPR tubes and stored in liquid nitrogen until use. The samples were (1) MF1(1,2) + Mn(II) with a protein:metal ratio of 1:0.8 (sample A), (2) MF1(1,2) + Mn(II) + ADP with a protein:metal:nucleotide ratio of 1:0.8:0.8 (sample C), (3) MF1(1,2) + Mn^{II}ADP with a protein:metal−nucleotide ratio of 1:2.4 (sample D), (4) MF1(0,0) + Mn(II) with a protein:metal ratio of 1:2.4 (sample E) [the sample MF1-(0,0) + Mn(II) with a protein:metal ratio of 1:0.8 was already studied in a previous investigation (sample B) and the results significant for the discussion of the present work will be briefly recalled], and (5) MF1(0,0) + ADP + Mn(II) with a protein:nucleotide:metal ratio of 1:10:2.4 (sample F).

EPR Measurements. The CW-EPR spectra were recorded at 20 K using an ELEXSYS Bruker spectrometer, equipped with a dielectric resonator, an Oxford CF935 liquid helium flow cryostat, and an Oxford ITC4 temperature controller. For some samples, the CW-EPR spectra were recorded also on an ECS106 instrument, equipped with a resonator TE_{102} and a liquid helium cryostat Oxford ESR900. A very low microwave power was used to avoid saturation.

Pulsed ESEEM experiments were carried out on the ELEXSYS Bruker spectrometer, equipped with the dielectric resonator. The measurements were performed at 5 K. The three-pulse ESEEM sequence was used to obtain the echo decays (*22*), and the proper phase cycle was applied to eliminate contributions from spurious echoes (*23*). The delay time τ between the first two pulses was chosen as 136 ns, unless specified, to minimize the free proton frequency signal. The time T between the second and third pulse was varied in steps of 8 ns, and 400 points were recorded, starting with the initial time $T_i = 80$ ns.

The recorded time decays were processed for dead time correction both with Mims's algorithm (*24*) and with the LPSVD method (*25*): both methods provided similar reconstructed spectra. The application of two different algorithms was used as a double check to verify the correctness of the reconstruction. After dead time reconstruction, the echo decays were Fourier transformed to produce ESEEM spectra in the frequency domain (FT-ESEEM spectra). We resorted to the frequency tracking method in the more complicated ESEEM spectra to reliably assign the peaks to ^{31}P, ^{1}H, or ^{14}N nuclei. In this method, FT-ESEEM spectra at different field positions are recorded: the nucleus giving rise to a particular signal can be assigned from the shift of the peak position with the magnetic field.

RESULTS

X-Band CW-EPR Spectra. In Figure 1 the X-band CW-EPR spectra recorded at $T = 20$ K of samples A−F are compared. For Mn(II) with $S = 5/2$, there are five fine structure transitions between the six electronic states, corresponding to $m_s = \pm 5/2$, $\pm 3/2$, and $\pm 1/2$. Each of these transitions are split into six lines by the hyperfine coupling to the ^{55}Mn nucleus ($I = 5/2$). In frozen solution the $m_s = -1/2 \leftrightarrow +1/2$ transition, which, to the first order, does not depend on the zero-field splitting (ZFS) parameters, is much more intense than the other fine structure transitions and gives rise to the familiar six-line pattern, dominating the

[1] Abbreviations: ADP, adenosine 5′-diphosphate; EDTA, ethylenediaminetetraacetic acid; EPR, electron paramagnetic resonance; ESEEM, electron spin echo envelope modulation; MF1(0,0), F1-H^+-ATPase from bovine heart mitochondria fully stripped; MF1(1,2) F1-H^+-ATPase from bovine heart mitochondria with tightly bound nucleotides; TF1, F1-H^+-ATPase from thermophilic *Bacillus* PS3; CF1, F1-H^+-ATPase from chloroplast.

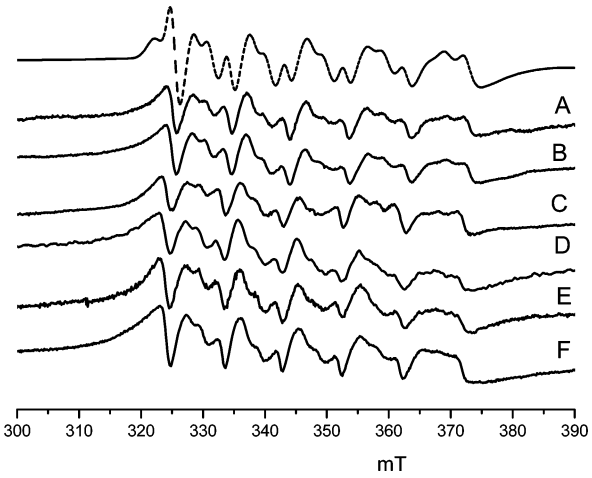

FIGURE 1: X-Band CW-EPR spectra of the six samples (traces A−F). The spectra, which were recorded at slightly different microwave frequencies, have been aligned to allow a better comparison. A simulation is included (first trace, dotted line, obtained by full Hamiltonian diagonalization). Experimental conditions: $T = 20$ K, microwave power 2 μW, modulation amplitude 0.5 mT. Simulation parameters: $D = 21$ mT, $E = 6$ mT, $A = 9.4$ mT.

powder spectrum. The other fine structure transitions result in a broad unresolved line shape mainly visible on the wings of the main spectrum. Between the six main peaks, small features appear, arising mainly from semiforbidden $\Delta M_I = \pm 1$ transitions that depend on the ZFS terms. From the EPR line shape, we can obtain information on the Mn(II) hyperfine coupling and on the ZFS parameters, D and E, that provide insight into the symmetry of the Mn(II) sphere (*26*). Large D values and E/D ratios are characteristic of less symmetric sites. Figure 1 also shows a calculated spectrum (first trace) obtained by a complete diagonalization of the spin Hamiltonian. The parameters used for the calculated spectrum are $|D| = 21 \pm 0.5$ mT (0.0196 cm^{-1}), $|E| = 6$ mT $\pm$ 0.5 (0.0056 cm^{-1}), and $A = 9.4$ mT.

The simulation could reasonably fit all the experimental spectra, which appear almost identical. This fact put in evidence that the metal site is very similar in all samples A−F and almost indistinguishable on the basis of the ZFS parameters. The ZFS parameters determined by the simulation are very close to the ZFS parameters obtained for other nucleotide-binding proteins containing the consensus P-loop motif (see ref *27* and references therein). In particular, as in our case, they all show large E/D values indicating a considerable deviation from the axial symmetry of the Mn(II) site. Instead, the relatively low D value indicates a small extent of the global distortion from the cubic symmetry (*26*).

MF1(1,2) + Mn(II) (1:0.8). Figure 2 shows the FT-ESEEM spectrum of sample A recorded at 328.0 mT: the spectrum presents strong peaks in the 0−5 MHz region. In particular, peaks at 1.55, 3.1, 3.55, 4.0, and 4.7 MHz are narrow and well resolved. These peaks can be ascribed to ^{14}N coordination to the Mn^{2+} ion. A detailed discussion of the ^{14}N ESEEM peaks for Mn(II) complexes is not feasible: for a spin system $S = 1/2$, $I = 1$ with mainly isotropic hyperfine coupling near the exact cancellation condition, the FT-ESEEM spectrum contains three sharp lines occurring at frequencies $\nu_+ = K(3 + \eta)$, $\nu_0 = 2K\eta$, and $\nu_- = K(3 - \eta)$ and a "double quantum" peak at the frequency $\nu_{dq} = 2[(\nu_I + a_{iso}m_s)^2 + K^2(3 + \eta)^2]^{1/2}$. The parameter K is $e^2qQ/(4h)$,

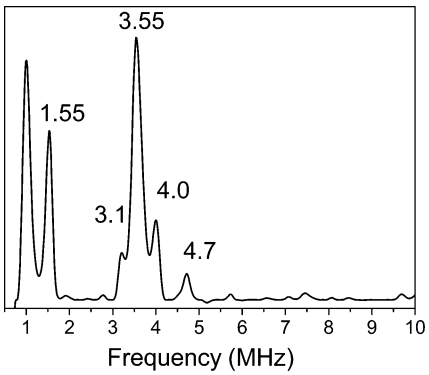

FIGURE 2: Three-pulse ESEEM of sample A, MF1(1,2) + Mn(II) (1:0.8) (field 328.0 mT, $\tau = 160$ ns).

where Q is the nitrogen quadrupole moment and q the electric field gradient at the nucleus ^{14}N, and η is the asymmetry parameter, $\eta = (Q_{xx} - Q_{yy})/Q_{zz}$, where Q_{xx}, Q_{yy}, and Q_{zz} are the principal values of the quadrupolar tensor (*28*, *29*). When the exact cancellation condition does not hold, the spectrum appears more complicated, due to anisotropic contributions making peaks broader and shifting peak frequencies (*30*). A more complicated situation occurs for a spin system with $S = 5/2$ and $I = 1$, where other peaks are possible, due to transitions from the outer electron spin manifolds (*31*). So far no detailed theoretical analysis has been done for the ESEEM spectra of an $S = 5/2$, $I = 1$ spin system; therefore, we will compare our spectra with literature results: Lee et al. (*32*) studied some Mn(II) complexes with Diocleinae lectins and obtained ESEEM spectra at a magnetic field of 325.8 mT with ^{14}N peaks at frequencies of 1.4−1.5, 3.3−3.4, and 4.8−5.0 MHz very similar to the peak positions of our spectrum. They attributed the pattern to histidine−Mn(II) coordination. McCracken et al. considered several imidazole−Mn(II) complexes, obtaining peaks at 1.4 and 3.5 MHz along with a peak from 4.9 to 5.3 MHz depending on the field setting (*33*): this latter peak, showing a slight shift with the field setting, was interpreted as the ^{14}N double quantum peak. Morrissey et al. (*34*), for Mn−GMP and Mn−ribozyme complexes, obtained ESEEM spectra at 360 mT, with peaks at 1.8 and 2.5−3.0 MHz along with the double quantum peak at 5.2 MHz. They attributed the pattern to Mn(II)−^{14}N interaction from N7 of the guanine. The issue of the identification of the nitrogen coordinated to the Mn^{2+} ion, from the ESEEM spectra, was undertaken by Tipton et al. (*35*) in a study on the Mn−tartrate dehydrogenase complex. Analysis of model complexes, aimed at distinguishing between different potential ligands, such as the ϵ-amino group of lysine or the imine nitrogen of imidazole from histidine, demonstrated that Mn−amino and Mn−imino complexes give rise to very similar ESEEM spectra. This was explained by considering that the quadrupole moment of free amino and imino nitrogens are often similar and the hcc of directly coordinated amino and imino nitrogens can be the same or very similar.

It is important to compare the ESEEM spectrum of Figure 2 (sample A**)** with the ESEEM spectrum reported in Figure 3 for the MF1(0,0) + Mn(II) (1:0.8) sample (sample B). This spectrum, widely discussed in a previous paper (*17*), shows only signals deriving from the interaction between Mn^{2+} and protons of directly coordinated water molecule(s). No low-frequency peaks attributable to ^{14}N interactions are present,

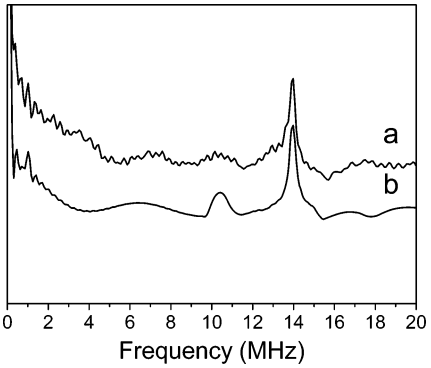

FIGURE 3: Three-pulse ESEEM of sample B, MF1(0,0) + Mn(II) (1:0.8): (a) experimental, (b) simulation performed including one proton coupled.

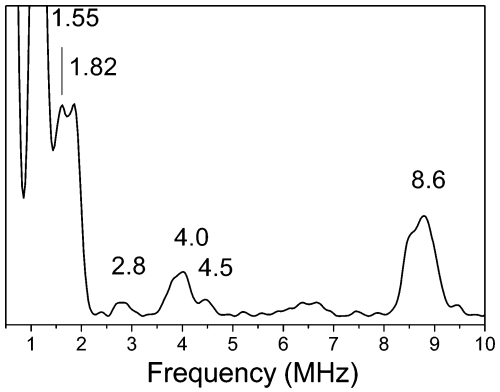

FIGURE 4: Three-pulse ESEEM of sample C, MF1(1,2) + Mn(II) + ADP (1:0.8:0.8) (field 357.2 mT).

as a clear indication that no Mn(II)−^{14}N coordination occurs in this sample.

MF1(1,2)+ Mn(II) + ADP (1:0.8:0.8). Sample C (Figure 4) was prepared by subsequently adding 0.8 equiv of ADP to sample A. This was done to verify that, when added to the protein in substoichiometric amount, Mn^{2+} enters into one of the catalytic sites. The rationale was that a substoichiometric amount of ADP binds to one of the catalytic sites, which are characterized by a much higher affinity with respect to the noncatalytic sites (*36*). Then, if ADP binds to the same site already occupied by Mn(II), this means that also substoichiometric Mn^{2+} binds to a catalytic site. Figure 4 shows the ESEEM spectrum at 357.2 mT and $\tau = 136$ ns: intense and narrow peaks are present at 1.55 and 1.82 MHz, along with broad and less intense resonances at 2.8 and 4.0 MHz with shoulders at 4.5 MHz, and less evident, at about 3.8 MHz. An intense and broad peak is evident at 8.6 MHz, which is attributable to ^{31}P coupling, on the basis of frequency tracking and of many literature data on protein-Mn(II) samples (*16*, *27*, *37*−*43*). The peaks at low frequency (1−3 MHz) do not move in a clear way with the magnetic field, supporting their assignment to quadrupolar peaks deriving from ^{14}N−Mn(II) interaction. The broad peak at 4.0 MHz probably contains contributions from the low-frequency component of the ^{31}P doublet and from ^{14}N signals. Therefore, we attribute the peaks in the range 1−3 MHz, a component of the peak centered at 4.0 MHz, and the shoulder at 4.5 MHz to the pattern deriving from the coordination of Mn^{2+} to a nitrogen nucleus. This pattern appears similar, but does not exactly overlay the ^{14}N pattern shown by sample A (see Figure 2).

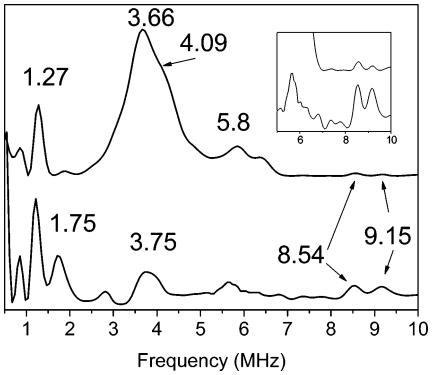

FIGURE 5: Three-pulse ESEEM of sample D, MF1(1,2) + Mn(II)ADP (1:2.4), at 367.6 mT: (upper trace) $\tau = 264$ ns, (lower trace) $\tau = 136$ ns. Inset: magnification of the zone 5−10 MHz to show the ^{31}P features.

The ^{31}P pattern (the doublet at about 4.0 and 8.6 MHz, with hyperfine splitting $a = 4.6$ MHz) is very similar to that normally found in the ESEEM spectra of Mn(II)−nucleotide complexes with ADP or ATP, both in model systems and in proteins (e.g., see Table 2 in ref *27*). In the case of a Mn(II)−ADP complex, the ^{31}P doublet derives from the phosphorus nucleus of the ADP β-phosphate group which is directly coordinated to the Mn^{2+} ion (*16*, *17*, *37*). This attribution is in accordance with the available MF1 crystal structures (*6*, *44*, *45*). The occurrence of phosphate binding shows that ADP is bound to the same site previously occupied by Mn(II), therefore identifying this site as a catalytic one.

MF1(1,2) + Mn^{II}ADP (1:2.4). ESEEM spectra of sample D, recorded at the same field setting (367.6 mT) with two different τ values (136 and 264 ns), are reported in Figure 5. The different τ values allow a more precise assignment of the ESEEM peaks. Both spectra contain two peaks at 8.5 and 9.15 MHz that shift with the magnetic field approximately as ^{31}P signals do. We attribute these peaks to the coupling of Mn(II) to the β-phosphate group of the coordinated ADP (see the results for sample C) and interpret the presence of two well-resolved signals as deriving from different ADP−Mn(II) interactions in the two filled metal sites. In principle, the splitting could derive also from the anisotropy of the hyperfine coupling. However, our interpretation is supported by considering that the ^{31}P signals are single peaks, without evident splittings, in all the ESEEM spectra present in the literature, showing coupling between Mn(II) and the ADP β-phosphate (*15*−*17*, *37*). In the few available HYSCORE spectra (*27*, *37*) the ^{31}P signals from ADP are largely isotropic and do not show the typical extension along the long axis of the line shape coming from a significant anisotropic interaction. The dipolar part of the Mn^{2+} interaction with ^{31}P of ADP in ATPase and GTPase has been inferred in refs *27*, *37*, and *40* from the peak broadening of the ESEEM and HYSCORE spectra. A maximum value of 0.9 MHz has been determined: this anisotropic contribution to the ^{31}P hyperfine coupling is not consistent with the presence of two features at 8.54 and 9.15 MHz observed in Figure 5.

The ^{31}P low-frequency signals are more clearly evident in the spectrum at $\tau = 264$ ns, where they are magnified with respect to the high-frequency pattern components. The suppression of the peaks at 8−9 MHz and amplification of

peaks at 3−4 MHz are further support of their identification as constituting a ^{31}P pattern. From the peak frequencies, we can estimate two different ^{31}P hyperfine couplings, $a_1 = 5.5 \pm 0.1$ and $a_2 = 4.4 \pm 0.1$ MHz, in the two filled metal sites. In principle, when Mn(II)ADP is added in stoichiometric excess with respect to the protein, the complex might occupy only the two vacant catalytic sites or in part the vacant catalytic sites and the vacant noncatalytic sites. However, the much higher affinity for nucleotides of the catalytic sites supports the first situation as the prevalent one (*36*). Slight differences in the coordination of the Mg^{2+} ions in the three catalytic sites (principally related to metal−ligand distances) have been observed also in the X-ray structures of bovine heart F1-ATPase (*5*), although in these structures no N-containing ligands have been identified (see the Discussion).

In the spectrum recorded with $\tau = 136$ ns, in the region 3−4 MHz, a single broad peak is evident at about 3.7 MHz. This peak should correspond to a ^{14}N peak superimposed onto the ^{31}P pattern, which is much less intense with this τ value.

In both spectra of Figure 5, there are features at low frequency: peaks at 1.27 and 1.8 ± 0.05 MHz are present in both spectra, and the peak at 2.8 MHz, present in the spectrum at $\tau = 136$ ns, is probably hidden by the intense ^{31}P resonance in the spectrum at 264 ns. These peaks, along with the broad resonance centered at about 5.9 MHz, are attributed to ^{14}N interaction on the basis of the weak frequency dependence on the magnetic field setting. This latter peak can be identified as the putative ^{14}N double quantum peak: it is significantly shifted at higher frequency with respect to the corresponding signals in other similar systems (see the results for samples A and C and previously reported literature examples). If we assume that the relationship $\nu_{dq} = 2[(\nu_I + a_{iso}m_s)^2 + K^2(3 + \eta)^2]^{1/2}$ holds also for an $S = 5/2$ system, the shift implies that a larger Mn(II)−^{14}N hyperfine interaction occurs in sample D with respect to samples A and C.

The double quantum peak appears structured (this is more evident in the spectrum at $\tau = 264$ ns), and this can be due to a more anisotropic ^{14}N coupling in sample D or, taking into account also the presence of two ^{31}P couplings, to a slightly different Mn(II)−nitrogen coordination in the two filled metal sites.

MF1(0,0)+ Mn(II) (1:2.4). Some experiments were performed on MF1 fully depleted of metal ions and nucleotides. This was done to clarify whether the different conformations of the catalytic sites, suggested by Figure 5, can be induced by binding the metal alone or by binding the Mn(II)−ADP substrate at two catalytic sites. When MF1(0,0) is loaded with 2.4 equiv of Mn^{2+} (sample E), we obtain the FT-ESEEM spectrum reported in Figure 6, which shows main peaks at 1.53, 3.65, and 5.75 MHz and a less intense signal at 2.20 MHz. Frequency tracking demonstrates that these signals constitute a ^{14}N pattern. The peaks at 1.55 and 3.65 MHz compare well with the corresponding peaks obtained for sample A, although in the case of sample E the signals are broader, and in particular the peak at 3.65 MHz is lacking any structure. The double quantum peak at 5.7 MHz is shifted to higher frequency if compared with the corresponding signal of sample A, but it is about at the same frequency as the double quantum peak of sample D. The peak is broad, but it does not appear structured.

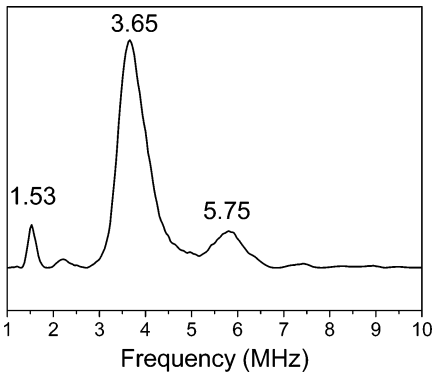

FIGURE 6: Three-pulse ESEEM of sample E, MF1(0,0) + Mn(II) (1:2.4) (field 324.6 mT).

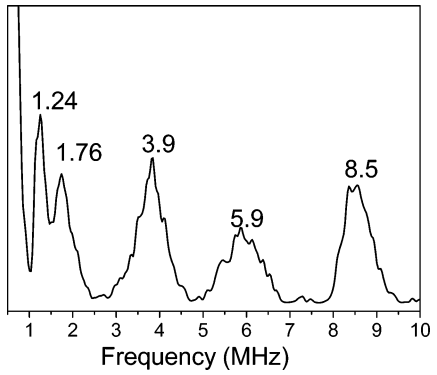

FIGURE 7: Three-pulse ESEEM of sample F, MF1(0,0) + ADP + Mn(II) (1:10:2.4), at 358.4 mT.

The comparison among the spectra of samples A, D, and E suggests that the nitrogen quadrupolar interaction is similar in samples E (Figure 6) and A (Figure 2), while the ^{14}N hyperfine coupling is definitely larger in sample E than in sample A and very close to that found in sample D (Figure 5). However, the ^{14}N pattern of sample E does not suggest the presence of distinct Mn(II)−nitrogen interactions occurring in the filled metal sites. This can be explained if ^{14}N coordination is established only in the second filled metal site. Alternatively, conformational changes can occur when MF1(0,0) is loaded with more than one Mn^{2+} equivalent, and these changes result in similar ^{14}N coordination in both the filled metal sites.

MF1(0,0) + ADP + Mn(II) (1:10:2.4). Sample F (Figure 7) has been prepared by preloading F1(0,0) with an excess of ADP and then adding Mn^{2+} in a protein:metal ratio of 1:2.4. Figure 7 shows the ESEEM spectrum recorded at 358.4 mT. The narrow signals at 1.24 and 1.76 MHz do not move with the magnetic field, while the broad peak at about 5.9 MHz has a small dependence on the field setting, supporting their assignment to quadrupolar and double quantum ^{14}N peaks. As in the previous samples, containing ADP, the peak at 8.5 MHz is attributed to the high-frequency component of the ^{31}P pattern deriving from the Mn(II)−ADP coordination. The 3.9 MHz peak could correspond to the low-frequency ^{31}P component, although it can take contribution from the ^{14}N feature generally found in the 3−4 MHz region (see the results for sample C). With this attribution, the ^{14}N pattern (1.24, 1.76, ∼3.9, and 5.9 MHz) is very similar to that shown by sample D. Furthermore, it has to be noted that the ^{14}N signals at lower frequencies are modified between samples E and F, i.e., upon ADP binding to MF1-

(0,0): this correlates well with the analogous modification of the ^{14}N pattern that occurs in sample A after ADP binding (sample C).

The ^{31}P signals do not show any evident splitting, as seen in the case of sample D. This result points to a very similar Mn(II)−ADP coordination in all of the filled metal sites. The lack of splitting of the ^{31}P peaks and the appearance of the ^{14}N pattern support the hypothesis that the two Mn(II) sites are structurally very similar, probably because, differently from sample D, the noncatalytic sites do not contain Mg(II)−ADP complexes, as only excess free ADP has been added to sample F.

DISCUSSION

In this paper we describe the spectroscopic properties of catalytic sites of F1-ATPase from bovine heart filled with Mn^{2+} added alone or as a metal−nucleotide complex. The occupancy of catalytic sites has been proved initially by the ESEEM spectrum obtained upon sequential addition of substoichiometric Mn^{2+} and ADP to MF1(1,2) that still contains endogenous nucleotides. This spectrum shows the occurrence of ^{31}P−Mn(II) interactions not observed when only Mn^{2+} was added (compare Figures 2 and 4). As the chelating properties of ADP versus Mn^{2+} are quite low (MaxChelator), thus avoiding the possibility that ADP caused Mn^{2+} dissociation/rebinding, we concluded that ADP binds to the same catalytic site previously occupied by Mn^{2+}. This approach has been successfully applied in our previous study, where we combined EPR spectroscopy and kinetic analyses (*17*). In fact, the kinetic measurements demonstrated that the sequential binding of substoichiometric Mn^{2+} and ADP occurs to a catalytic site of MF1(0,0), and this matched the occurrence of ^{31}P−Mn(II) interactions in the ESEEM spectrum. This provided a tool to identify catalytic sites. Filling of catalytic sites occurred also in MF1(1,2) incubated with 2.4 equiv of Mn(II)−ADP complex, due to the much higher affinity for nucleotides of the catalytic sites (*36*). Similarly, incubation of MF1(0,0) with 2.4 equiv of Mn^{2+} induced metal ion binding most probably to catalytic sites (samples E and F). In fact, from the literature, it is known that metal ions bind to noncatalytic sites only in the presence of large metal−nucleotide excess, like in MF1 crystals (*4*−*6*, *19*). We underline that all the samples are characterized by almost identical CW-EPR spectra, supporting that they originate from a unique kind of Mn^{2+} center. On the other hand, different ESEEM spectra are obtained, but all of them show ^{14}N coordination to Mn(II) when more than one metal ion is present in the protein.

This finding is apparently in contrast to the available X-ray structures of bovine F1-ATPase. In the inhibited forms with ADP and beryllium fluoride (*6*) or aluminum fluoride (*44*) there is evidence that Mg^{2+} binds: the oxygen of the β-Thr163 hydroxyl group; three water molecules H-bonded to β-Glu192 and β-Asp256; the β-phosphate oxygen of the bound nucleotide; a fluorine ion mimicking the oxygen of the released phosphate. The more recent ground-state structure (*45*) confirmed that γ-P oxygen completed the octahedral coordination. Nevertheless, Buy et al. obtained an ESEEM pattern indicative of a ^{14}N−metal interaction (peaks at 1.8, 3.1, and 4.85 MHz at a magnetic field of 346.0 mT) on a sample of TF1 (F1 from thermophilic bacterium *Bacillus* PS3) loaded with Mn^{2+} (TF1:Mn(II) = 1:0.4) (*16*). These authors proposed that, in the absence of nucleotides, Mn(II) is coordinated to the ϵ-amino group of the β-Lys162 (bovine numbering), which is perhaps replaced by the γ-phosphate of ATP upon nucleotide binding (although their data were not conclusive). Our results show that ADP binding does not replace ^{14}N in the coordination sphere of Mn(II), supporting the hypothesis that a N donor occurs in the absence of γ-phosphate oxygen. In fact, in the closed conformations of the β subunit found in the crystal structures of MF1, β-Lys162 is involved in γ-phosphate charge stabilization; instead, in the empty β subunit, β-Lys162 adopts an extended conformation, able to bind the catalytic substrates. However, also the guanidine groups of β-Arg189 and α-Arg 373 are localized very near the Mg^{2+} ion and interact with γ-phosphate in the closed conformations of β subunits. In addition, all these residues are important in the catalytic process, and their side chains move significantly during catalysis. Two other nonbackbone nitrogens, localized within a 6 Å radius from the Mg^{2+} ion, are those of β-Arg260 and β-Asn257. Different backbone nitrogens could potentially be ligands of Mn(II), such as β-Val164, β-Lys162, and β-Thr163. Nevertheless, the similarity between the ESEEM spectra of different Mn(II) complexes containing ^{14}N ligands reported in the literature (see previous comments) does not allow the ^{14}N signals of our spectra to be attributed to a specific amino acidic residue.

The main result of our work is the finding that the first Mn^{2+} cation added to the "less structurally constrained" fully depleted MF1(0,0) has the same structural effect as the endogenous Mg−ADP complex bound to the high-affinity catalytic site in the "more structurally constrained" MF1-(1,2). In fact, ESEEM spectra of MF1(0,0) loaded with 2.4 equiv of Mn^{2+} and of MF1(1,2) loaded with 0.8 equiv of Mn^{2+} evidenced similar ^{14}N coordination of the metal cation. On the other hand, ESEEM spectra of MF1(0,0) loaded with 0.8 equiv of Mn(II) showed no evidence of metal−nitrogen interaction (*17*). The pivotal role of the metal ion in shaping the catalytic site was further evidenced by the observation that the nitrogen−metal coordination was not altered in the sample obtained by adding to MF1(0,0) an excess of free ADP and afterward 2.4 equiv of Mn^{2+}. These results indicate that different Mn(II) coordinations exist in the first and second metal sites, at least when sequential ion loading is performed. These two sites might correspond to the two tight-binding sites for Mg^{2+} originally characterized in beef heart F1-ATPase, where metal ions were not necessarily bound in association with nucleotides (*46*). Mg^{2+} in these sites appeared to play fundamental roles: in fact, filling of the first site was necessary to avoid the enzyme depolymerization, while the following binding of Mg^{2+} to the second site induced a parallel increase of the enzyme activity. Such properties suggest different structural effects, in accordance with our data which put into evidence different interactions with the surrounding amino acid residues.

In conclusion, the ESEEM technique appears to be a very sensitive and suitable spectroscopic method for conformational studies of MF1, after replacement of the naturally occurring Mg^{2+} cation with the paramagnetic Mn^{2+}. The use of EPR techniques made possible observation of the protein rearrangements induced by the added metal or metal−ADP complex, with the advantage of using the protein in frozen

solutions. Crystal structures of MF1 showed that the binding of the substrate to the β subunit empty of nucleotide has a dramatic effect on its conformation: there is a 16° rotation of the C-terminal domain that results in a partial closing of the interface between the β subunit and the neighboring α subunit, allowing the cyclic interconversion of the sites. Even relatively small structural differences at the catalytic sites have a marked effect on catalysis, as evidenced by mutation of a catalytic carboxylate in TF1 (*47*). We cannot define the structural changes induced by Mn^{2+} binding, nor can we refer to a specific β conformation observed in MF1 crystal structures. In fact, the filling of the six nucleotide sites by metal−nucleotide complexes in our preparations is different from that of the crystallized protein. Nevertheless, our results clearly show that the metal alone is able to shape the catalytic sites as the Mg−nucleotide complex.

ACKNOWLEDGMENT

We are very grateful to Prof. A. E. Senior (University of Rochester Medical Center, Rochester, NY) for helpful discussions and suggestions.

REFERENCES

1. Noji, H., Yasuda, R., Yoshida, M., and Kinosita, K. (1997) Direct observation of the rotation of F1-ATPase, *Nature 386*, 299−302.
2. Diez, M., Zimmerman, B., Börsch, M., König, M., Schweinberger, E., Steigmiller, S., Reuter, R., Felekyan, S., Kudryavtsev, V., Seidel, P., and Gräber, P. (2004) Proton-powered subunit rotation in single membrane-bound F0F1-ATP synthase, *Nat. Struct. Mol. Biol. 11*, 135−141.
3. Itoh, H., Takahashi, A., Adachi, K., Noji, H., Yasuda, R., Yoshida, M., and Kinosita, K. (2004) Mechanically driven ATP synthesis by F1-ATPase, *Nature 427*, 465−468.
4. Abrahams, J. P., Leslie, A. G. W., Lutter, R., and Walker, J. E. (1994) Structure at 2.8 Å resolution of F1-ATPase from bovine heart mitochondria, *Nature 370*, 621−628.
5. Menz, R. I., Walker, J. E., and Leslie, A. G. W. (2001) Structure of bovine mitochondrial F1-ATPase with nucleotide bound to all three catalytic sites: Implications for the mechanism of rotary catalysis, *Cell 106*, 331−341.
6. Kagawa, R., Montgomery, M-G., Braig, K., Leslie, A. G. W., and Walker, J. E. (2004) The structure of bovine F_1-ATPase inhibited by ADP and beryllium fluoride, *EMBO J. 23*, 2734−2744.
7. Boyer, P. D. (1993) The binding change mechanism for ATP synthase-some probabilities and possibilities, *Biochim. Biophys. Acta 1140*, 215−250.
8. Senior, A. E., Nadanaciva, S., and Weber, J. (2002) The molecular mechanism of ATP synthesis by F1F0-ATP synthase, *Biochim. Biophys. Acta 1553*, 188−211
9. Milgrom, Y. M., and Cross, R. L. (2005) Rapid hydrolysis of ATP by mitochondrial F1-ATPase correlates with the filling of the second of three catalytic sites, *Proc. Natl. Acad. Sci. U.S.A. 102*, 13831−13836.
10. Weber, J., Wilke-Mounts, S., Lee, R. S., Grell, E., and Senior, A. E. (1993) Specific placement of tryptophan in the catalytic sites of Escherichia coli F1-ATPase provides a direct probe of nucleotide binding: maximal ATP hydrolysis occurs with three sites occupied, *J. Biol. Chem. 268*, 20126−20133.
11. Weber, J., Wilke-Mounts, and Senior, A. E. (1994) Cooperativity and stoichiometry of substrate binding to the catalytic sites of Escherichia coli F1-ATPase, *J. Biol. Chem. 269*, 20462−20467.
12. Kironde, F. A. S., and Cross, R. L. (1986) Adenine nucleotide-binding sites on beef heart F1-ATPase, *J. Biol. Chem. 261*, 12544−12549.
13. Frasch, W. D. **(**2000) The participation of metals in the mechanism of the F1-ATPase, *Biochim. Biophys. Acta 1458* (2, 3), 310−25.
14. Chen, W., Hu, C. Y., Crampton, D. J., and Frasch, W. D. (2000) Characterization of the metal binding environment of catalytic site 1 of chloroplast F1-ATPase from *Chlamydomonas*, *Biochemistry 39* (31), 9393−400.
15. Zimmermann, J. L., Schneider, B., Morlet, S., Amano, T., and Sigalat, C. (2000) The role of the Mg^{2+} cation in ATP synthase studied by electron paramagnetic resonance using VO^{2+} and Mn^{2+} paramagnetic probes, *Spectrochim. Acta, Part A 56* (2), 285−99.
16. Buy, C., Girault, G., and Zimmermann, J. L. (1996) Metal binding sites of H+-ATPase from chloroplast and *Bacillus* PS3 studied by EPR and pulsed EPR spectroscopy of bound manganese(II), *Biochemistry 35* (30), 9880−91.
17. Zoleo, A., Contessi, S., Lippe, G., Pinato, L., Brustolon, M., Brunel, Λ.X., Dabbeni-Sala, F., and Maniero, A. L. (2004) High-affinity metal-binding site in beef heart mitochondrial F1ATPase: An EPR spectroscopy study, *Biochemistry 43*, 13214−24.
18. Horstman, L. L., and Racker, E. (1970) Partial resolution of the enzyme catalyzing oxidative phosphorylation. XXII. Interaction between mitochondrial adenosine triphosphatase inhibitor and mitochondrial adenosine triphosphatase, *J. Biol. Chem. 245*, 1336−44.
19. Lutter, R., Abrahams, J. P., van Raaij, M. J., Todd, R. J., Lundqvist, T., Buchana, S. K., Leslie, A. G. W., and Walker, J. E. (1993) Crystallization of F1-ATPase from bovine heart mitochondria, *J. Mol. Biol. 229*, 787−90.
20. Di Pietro, A., Penin, F., Julliard, J. H., Godinot, C., and Gautheron, D. C. (1988) IF_1 inhibition of mitochondrial F_1-ATPase is correlated to entrapment of four adenine- or guanine-nucleotides including at least one triphosphate, *Biochem. Biophys. Res. Commun. 152*, 1319−25.
21. Laemmli, U. K. (1970) Cleavage of structural proteins during the assembly of the head of bacteriophage T4, *Nature 277*, 680−85.
22. Mims, W. B. (1972) Envelope modulation in spin-echo experiments, *Phys. Rev. B 5* (7), 2409−19.
23. Fauth, J. M., Schweiger, A., Braunschweiler, L., Forrer, J., and Ernst, R. R. (1986) Elimination of unwanted echoes and reduction of dead time in three-pulse electron spin-echo spectroscopy, *J. Magn. Reson. 66*, 74−85.
24. Mims, W. B. (1984) Elimination of the dead-time artifact in electron spin-echo envelope spectra, *J. Magn. Reson. 59*, 291−306.
25. Barkhuijsen, H., de Beer, R., Bovée, W. M. M. J., and van Ormondt, D. (1985) Retrieval of frequencies, amplitudes, damping factors, and phases from time-domain signals using a linear least-squares procedure, *Magn. Reson. 61*, 465−81.
26. Reed, G. H., and Markham, G. D. (1984) EPR of Mn(II) Complexes with Enzymes and Other Proteins, in *Biological Magnetic Resonance* (Berliner, L. J., and Reuben, J., Eds.) Vol. 6, pp 73−142, Plenum Press, New York.
27. Petersen, J., Gessner, C., Fischer, K., Mitchell, C. J., Lowe, D. J., and Lubitz, W. (2005) Mn^{2+}-adenosine nucleotide complexes in the presence of the nitrogenase-iron protein: detection of conformational rearrangements directly at the nucleotide binding site by EPR and 2D-ESEEM (two-dimensional electron spin-echo envelope modulation spectroscopy), *Biochem. J. 391*, 527−39.
28. Mims, W. B., and Peisach, J. (1978) The nuclear modulation effect in electron spin echoes for complexes of Cu^{2+} and imidazole with ^{14}N and ^{15}N, *J. Chem. Phys. 69*, 4921−30.
29. Flanagan, H. L., and Singel, D. J. (1987) Analysis of ^{14}N ESEEM patterns of randomly oriented solids, *J. Chem. Phys. 87*, 5606−16.
30. Dikanov, S. A., and Tsvetkov, D. Yu. (1992) *Electron spin echo envelope modulation (ESEEM) spectroscopy*, CRC Press, Boca Raton, FL.
31. Hoogstraten, C. G., Grant, C. V., Horton, T. E., DeRose, V. J., and Britt, R. D. (2002) Structural analysis of metal ion ligation to nucleotides and nucleic acids using pulsed EPR spectroscopy, *J. Am. Chem. Soc., 124* (5), 834−42.
32. Lee, H. C., Goroncy, A. K., Peisach, J., Cavada, B. S., Grangeiro, T. B., Ramos, M. V., Sampaio, A. H., Dam, T. K., and Brewer, F. C. (2000) Demonstration of a conserved histidine and two water ligands at the Mn^{2+} site in diocleinae lectins by pulsed EPR spectroscopy, *Biochemistry 39*, 2340−46.
33. McCracken, J., Peisach, J., Bhattacharyya, L., and Brewer, F. (1991) Electron spin echo enevelope modulation studies of lectins: Evidence for a conserved Mn^{2+}-binding site, *Biochemistry 30*, 4486−91.
34. Morrissey, S. R., Horton, T. E., Grant, C. V., Hoogstraten, C. G., Britt, R. D., and DeRose, V. J. (1999) Mn^{2+}-nitrogen interactions in RNA probed by electron spin-echo envelope modulation spectroscopy: Application to the hammerhead ribozyme, *J. Am. Chem. Soc. 121* (39), 9215−18.

35. Tipton, P. A., and Peisach, J. (1991) Pulsed EPR analysis of tartrate dehydrogenase active-site complexes, *Biochemistry 30*, 739−44
36. Jault, J. M., and Allison, W. S. (1993) Slow binding of ATP to noncatalytic nucleotide binding sites which accelerates catalysis is responsible for apparent negative cooperativity exhibited by the bovine mitochondrial F1-ATPase, *J. Biol. Chem. 268*, 1558−66.
37. Schneider, B., Sigalat, C., Amano, T., and Zimmermann, J. L. (2000) Evidence for changes in the nucleotide conformation in the active site of H^+-ATPase as determined by pulsed EPR spectroscopy, *Biochemistry 39*, 15500−12.
38. Lo Brutto, R., Smithers, G. W., Reed, G. H., Orme-Johnson, W. H., Tan, S. L., and Leigh, J. S., Jr. (1986) Observation of manganese(II)-ligand superhyperfine couplings in complexes with proteins by electron spin-echo spectroscopy, *Biochemistry 25*, 5654−60.
39. Serpesu, E. H., McCracken, J., Peisach, J., and Mildvann, A. S. (1988) Electron Spin Echo Modulation and nuclear relaxation studies of staphylococcal nuclease and its metal coordinating mutants, *Biochemistry 27*, 8024−44.
40. Larsen, R. G., Halkides, C. J., Redfield, A. J., and Singel, D. J. (1992) Electron spin echo envelope modulation spectroscopy of Mn^{2+}GDP complexes of N-*ras* p21 with selective ^{15}N labeling, *J. Am. Chem. Soc. 114*, 9608−11.
41. Larsen, R. G., Halkides, C. J., and Singel, D. J. (1993) A geometric representation of nuclear modulation effects: the effects of high electron spin multeplicity on the electron spin echo envelope modulation spectra of Mn^{2+} complexes of N-*ras* p21, *J. Chem. Phys. 98*, 6704−6721.
42. Halkides, C. J., Farrar, C. T., Larsen, R. G., Redfield, A. G., and Singel, D. J. (1994) Characterization of the active site of p21 *ras* by electron spin-echo envelope modulation spectroscopy with selective labeling: comparison between GDP and GTP forms, *Biochemistry 33*, 4019−4035.
43. Lagler, P. M., Lee, H. C., Peisach, J., and Mildvan, A. S. (2002) Kinetic and magnetic resonances studies of the role of metal ions in the mechanism of *Escherichia choli* GDP-mannose mannosyl hydrolase, an unusual nudics enzyme, *Biochemistry 41*, 4655−4668.
44. Braig, K, Menz, R. I., Montgomery, M. G., Leslie, A. G. W., and Walker, J. E. (2000) Structure of bovine mitochondrial F1-ATPase inhibited by Mg2+ADP and aluminium fluoride, *Structure 8* (6), 567−573.
45. Bowler, M. W., Montgomery, M. G., Leslie, A. G., and Walker J. E. (2007) Ground state structure of F1-ATPase from bovine heart mitochondria at 1.9 Å resolution, *J. Biol. Chem.* (in press).
46. Senior, A. E., Richardson, L. V., Baker, K., and Wise, J. G. (1980) Tight divalent cation-binding sites of soluble adenosine triphosphatase (F1) from beef heart mitochondria and Escherichia coli, *J. Biol. Chem. 255*, 7211−17.
47. Amano, T., Tozawa, K., Yoshida, M., and Murakami, H. (1994) Spatial precision of a catalytic carboxylate of F1-ATPase beta subunit probed by introducing different carboxylate-containing side chains, *FEBS Lett. 348*, 93−98.

BI700949E